5390 *Organometallics* **2010,** *29,* 5390–5401
DOI: 10.1021/om100395r

ORGANOMETALLICS
Article

Comparison of Cobalt and Nickel Complexes with Sterically Demanding Cyclic Diphosphine Ligands: Electrocatalytic H_2 Production by $[Co(P^{tBu}{}_2N^{Ph}{}_2)(CH_3CN)_3](BF_4)_2$†

Eric S. Wiedner,‡ Jenny Y. Yang,‡ William G. Dougherty,§ W. Scott Kassel,§ R. Morris Bullock,‡ M. Rakowski DuBois,‡ and Daniel L. DuBois*,‡

‡*Chemical and Materials Sciences Division, Pacific Northwest National Laboratory, P.O. Box 999, K2-57, Richland, Washington 99352, and* §*Department of Chemistry, Villanova University, Villanova, Pennsylvania 19085*

Received April 30, 2010

The cyclic diphosphine ligands $P^{tBu}{}_2N^{Ph}{}_2$ and $P^{tBu}{}_2N^{Bz}{}_2$ have been synthesized and used to prepare new complexes of Co(II) and Ni(II) with the formula $[M(P^{tBu}{}_2N^{R}{}_2)(CH_3CN)_n](BF_4)_2$ ($n = 2, 3$). The products have been characterized by variable-temperature NMR data, X-ray diffraction studies, and cyclic voltammetry, and properties of the new complexes have been compared with those of previously studied complexes containing $P^{Ph}{}_2N^{R}{}_2$ ligands. The variation of either phosphorus or nitrogen substituents in these ligands can result in significant differences in the structure, electrochemistry, and reactivity of the metal complexes. $[Co(P^{tBu}{}_2N^{Ph}{}_2)(CH_3CN)_3](BF_4)_2$ is found to be an effective electrocatalyst for the formation of hydrogen using bromoanilinium tetrafluoroborate as the acid, with a turnover frequency of 160 s^{-1} and an overpotential of 160 mV. These cobalt derivatives are a promising class of catalysts for further study and optimization.

Introduction

The electrocatalytic reduction of protons to produce hydrogen is the simplest fuel generation reaction. This reaction has potential technological importance in the storage of the electrical energy produced using renewable energy sources such as solar and wind, which exhibit significant temporal variations. Although platinum is an excellent catalyst for this reaction, its high cost and low abundance have stimulated the search for alternatives. The high catalytic activity of [NiFe] and [FeFe] hydrogenase enzymes clearly demonstrate that the use of noble metals is not required for H_2 production and oxidation.[1−6] These considerations have resulted in the development of a variety of molecular catalysts, including FeS dimers,[7−11] $CpMoS_2$ dimers,[12] and cobalt macrocycles.[13−15]

Efforts in our laboratories have focused primarily on the design of H_2 oxidation and production catalysts that involve first-row transition-metal complexes containing diphosphine ligands with pendant bases.[16,17] In our comparisons of nickel and cobalt complexes with $P^{R}{}_2N^{R'}{}_2$ ligands, such as those shown in **1**, we have found different and complementary structural requirements for catalytic activity. Nickel complexes incorporating two $P^{R}{}_2N^{R'}{}_2$ ligands are fast and efficient catalysts for H_2 production (**1a**) and for H_2 oxidation (**1b**).[18,19] The studies showed that ligand substituents markedly alter the affinities of the complexes for H_2 addition and control the bias of the catalyst for oxidation or

† Part of the Dietmar Seyferth Festschrift. This paper is dedicated to Dietmar Seyferth, in honor and appreciation for his decades of service as Editor of Organometallics.

(1) Frey, M. *ChemBioChem* **2002**, *3*, 153–160.
(2) Peters, J. W. *Curr. Opin. Struct. Biol.* **1999**, *9*, 670–676.
(3) Peters, J. W.; Lanzilotta, W. N.; Lemon, B. J.; Seefeldt, L. C. *Science* **1998**, *282*, 1853–1858.
(4) Nicolet, Y.; de Lacey, A. L.; Vernède, X.; Fernandez, V. M.; Hatchikian, E. C.; Fontecilla-Camps, J. C. *J. Am. Chem. Soc.* **2001**, *123*, 1596–1601.
(5) Fontecilla-Camps, J. C.; Volbeda, A.; Cavazza, C.; Nicolet, Y. *Chem. Rev.* **2007**, *107*, 4273–4303.
(6) Armstrong, F. A.; Belsey, N. A.; Cracknell, J. A.; Goldet, G.; Parkin., A.; Reisner, E.; Vincent, K. A.; Wait, A. F. *Chem. Soc. Rev.* **2009**, *38*, 38–51.
(7) Pickett, C. J.; Best, S. P. *Coord. Chem. Rev.* **2005**, *249*, 1517–1690.
(8) (a) Barton, B. E.; Olsen, M. T.; Rauchfuss, T. B. *J. Am. Chem. Soc.* **2008**, *130*, 16834–16835. (b) Gloaguen, F.; Rauchfuss, T. B. *Chem. Soc. Rev.* **2009**, *38*, 100–108.
(9) (a) Liu, T.; Darensbourg, M. Y. *J. Am. Chem. Soc.* **2007**, *129*, 7008–7009. (b) Tye, J. W.; Darensbourg, M. Y.; Hall, M. B. *Inorg. Chem.* **2008**, *47*, 2380–2388.
(10) Löscher, S.; Schwartz, L.; Stein, M.; Ott, S.; Haumann, M. *Inorg. Chem.* **2007**, *46*, 11094–11105.
(11) Felton, G. A. N.; Petro, B. J.; Glass, R. S.; Lichtenberger, D. L.; Evans, D. H. *J. Am. Chem. Soc.* **2009**, *131*, 11290–11291.
(12) Appel, A. M.; DuBois, D. L.; Rakowski DuBois, M. *J. Am. Chem. Soc.* **2005**, *127*, 12717–12726.
(13) (a) Jacques, P.-A.; Vincent Artero, V.; Pécaut, J.; Fontecave, M. *Proc. Natl. Acad. Sci. U.S.A.* **2009**, *106*, 20627–20632. (b) Artero, V.; Fontecave, M. *Coord. Chem. Rev.* **2005**, *249*, 1518–1535.
(14) (a) Berben, L. A.; Peters, J. C. *Chem. Commun.* **2010**, *46*, 398–400. (b) Hu, X.; Brunschwig, B. S.; Peters, J. C. *J. Am. Chem. Soc.* **2007**, *129*, 8988–8998.
(15) Connolly, P.; Espenson, J. H. *Inorg. Chem.* **1986**, *25*, 2684–2688.
(16) (a) Rakowski DuBois, M.; DuBois, D. L. *Chem. Soc. Rev.* **2009**, *38*, 62–72. (b) Rakowski DuBois, M.; DuBois, D. L. *C. R. Chim.* **2008**, *11*, 805–817. (c) Rakowski DuBois, M.; DuBois, D. L. *Acc. Chem. Res.* **2009**, *42*, 1974–1982.
(17) Curtis, C. J.; Miedaner, A.; Ciancanelli, R. F.; Ellis, W. W.; Noll, B. C.; Rakowski DuBois, M.; DuBois, D. L. *Inorg. Chem.* **2003**, *42*, 216–227.

 Published on Web 08/31/2010

reduction.[20] The closely related nickel complex $[Ni(P^{Ph}{}_2N^{Bz}{}_2)(dppp)](BF_4)_2$ (where dppp is bis(diphenylphosphino)propane), which contains only one base positioned near the metal center, is a much poorer catalyst for H_2 oxidation than **1b**, despite a stronger thermodynamic driving force for H_2 addition.[21] We therefore concluded that two bases positioned near the active metal site were important for catalytic activity in the Ni bis(diphosphine) systems. However, in these previous studies with $P^{Ph}{}_2N^{R'}{}_2$ ligands, we were unable to examine the effect on catalytic activity of other ligands in nickel complexes of the type $[Ni(P^{Ph}{}_2N^{R'}{}_2)L_n](BF_4)_2$ ($n = 2, 3$) because of difficulties in their synthesis. For example, the addition of 1 equiv of $P^{Ph}{}_2N^{Ph}{}_2$ to $[Ni(CH_3CN)_6](BF_4)_2$ resulted in the formation of $^1/_2$ equiv of the known bis(diphosphine) complex **1a** rather than the desired mixed ligand derivative.[22]

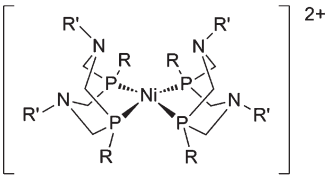

1a R = Ph, R' = Ph
1b R = Cy, R' = Bz

In our studies of cobalt complexes with $P^{Ph}{}_2N^{Ph}{}_2$ ligands we found that the syntheses of products containing either one or two cyclic ligands were readily achieved by controlling ligand stoichiometry in the syntheses.[22] The complex $[Co(P^{Ph}{}_2N^{Ph}{}_2)_2(CH_3CN)](BF_4)_2$ was isostructural with the active nickel catalyst **1a**. However, the cobalt product was not an electrocatalyst for H_2 formation because of the facile dissociation of one $P^{Ph}{}_2N^{Ph}{}_2$ ligand in the presence of acid. In contrast, $[Co(P^{Ph}{}_2N^{Ph}{}_2)(CH_3CN)_3](BF_4)_2$, with a single base positioned near the cobalt center, was stable to excess acid and performed as an effective electrocatalyst for hydrogen formation with a rate and overpotential similar to those of **1a**.

In this paper we describe the syntheses and characterizations of the new cyclic ligands $P^{tBu}{}_2N^{Ph}{}_2$ and $P^{tBu}{}_2N^{Bz}{}_2$ and their nickel and cobalt complexes. Introduction of the sterically demanding and electron-donating *tert*-butyl substituent on phosphorus might be expected to affect the stoichiometry of the ligand additions, cause structural distortions in the resulting complexes, and influence the reduction potentials at the metal centers. We report here how these effects are manifested in the nickel and cobalt derivatives, and we investigate the factors that promote high electrocatalytic activity for one of the new cobalt derivatives, while the other new complexes were found to be catalytically inactive.

Results

Synthesis and Characterization of Ligands. The two new cyclic diphosphine ligands $P^{tBu}{}_2N^{Ph}{}_2$ and $P^{tBu}{}_2N^{Bz}{}_2$ were prepared by first reacting *tert*-butylphosphine with paraformaldehyde to form bis(hydroxymethyl)-*tert*-butylphosphine followed by reaction with 1 equiv of either aniline or benzylamine in hot ethanol. The desired ligands precipitate as white solids upon cooling, and subsequent workup produces the desired ligands in reasonable yields and high purity. An interesting feature of these new ligands is the observation of conformational isomers in the variable-temperature NMR spectra. Furthermore, the two ligands, which differ only by the presence of phenyl or benzyl substituents on the nitrogens, show significantly different fluxional properties.

At room temperature $P^{tBu}{}_2N^{Ph}{}_2$ exists as two discrete isomers which each display a pair of mutually coupled methylene protons (NCH_2P) in the ^1H NMR spectrum. The two-bond proton−phosphorus coupling constant ($^2J_{HP}$) for each NCH_2P resonance was determined through selective homonuclear decoupling experiments. By comparison of $^2J_{HP}$ with literature values,[23] each isomer was determined to possess both an axial PCH_2N proton (H_{ax}, $^2J_{HP} = 4.7$ or 5.4 Hz) and an equatorial PCH_2N proton (H_{eq}, $^2J_{HP} = 14.8$ Hz). In the 2D NOESY spectrum of $P^{tBu}{}_2N^{Ph}{}_2$, both isomers displayed a cross-peak between the resonance of the ortho hydrogens of NPh (H_{ortho}) and the H_{eq} resonances (see Figure S1 in the Supporting Information). However, only one isomer displayed a NOESY cross-peak between the H_{ortho} and H_{ax} resonances. Therefore, the isomers were assigned as "crown" and "saddle" conformers, with the "saddle" conformer possessing a NOESY cross-peak between H_{ortho} and H_{ax}. This conformer assignment was supported by MM2 calculations through determination of the average H_{ortho} and H_{ax} distances, which were found to be 3.5 Å ("crown") and 1.9 Å ("saddle"). No peak coalescence was observed in the ^1H NMR spectrum of $P^{tBu}{}_2N^{Ph}{}_2$ up to 80 °C in CD_3CN, indicating that conformational exchange is slow for this molecule. Models indicate that the phenyl ring is restricted in its orientation, resulting in a relatively high energy barrier for rearrangement.

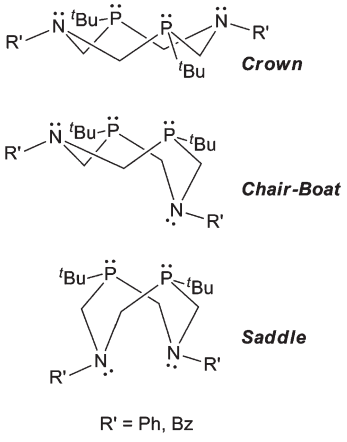

R' = Ph, Bz

For the second ligand, $P^{tBu}{}_2N^{Bz}{}_2$, the PCH_2N methylene protons are equivalent on the NMR time scale at room temperature, indicating fast exchange between conformations under these conditions. The benzyl and methylene resonances begin to decoalesce at 0 °C in THF-d_8. At −50 °C, two conformers of $P^{tBu}{}_2N^{Bz}{}_2$ are observed clearly in

(18) Wilson, A. D.; Newell, R. H.; McNevin, M. J.; Muckerman, J. T.; Rakowski DuBois, M.; DuBois, D. L. *J. Am. Chem. Soc.* **2006**, *128*, 358–366.
(19) Wilson, A. D.; Miedaner, A.; Muckerman, J. T.; DuBois, D. L.; Rakowski DuBois, M. *Proc. Natl. Acad. Sci. U.S.A.* **2007**, *104*, 6951–6956.
(20) Fraze, K.; Wilson, A. D.; Appel, A. M.; Rakowski DuBois, M.; DuBois, D. L. *Organometallics* **2007**, *26*, 5003–5009.
(21) Yang, J. Y.; Bullock, R. M.; Shaw, W. J.; Twamley, B.; Fraze, K.; Rakowski DuBois, M.; DuBois, D. L. *J. Am. Chem. Soc.* **2009**, *131*, 5935–5945.
(22) Jacobsen, G. M.; Yang, J.; Twamley, B.; Wilson, A. D.; Bullock, R. M.; Rakowski DuBois, M.; DuBois, D. L. *Energy Environ. Sci.* **2008**, *1*, 167–174.
(23) (a) Märkl, V. G.; Jin, G. Y.; Schoerner, C. *Tetrahedron Lett.* **1980**, *21*, 1409–1412. (b) Albrand, J. P.; Gagnaire, D.; Robert, J. B. *Chem. Commun.* **1968**, 1469–1470. (c) Albrand, J. P.; Gagnaire, D.; Picard, M.; Robert, J. B. *Tetrahedron Lett.* **1970**, *11*, 4593–4596.

Scheme 1

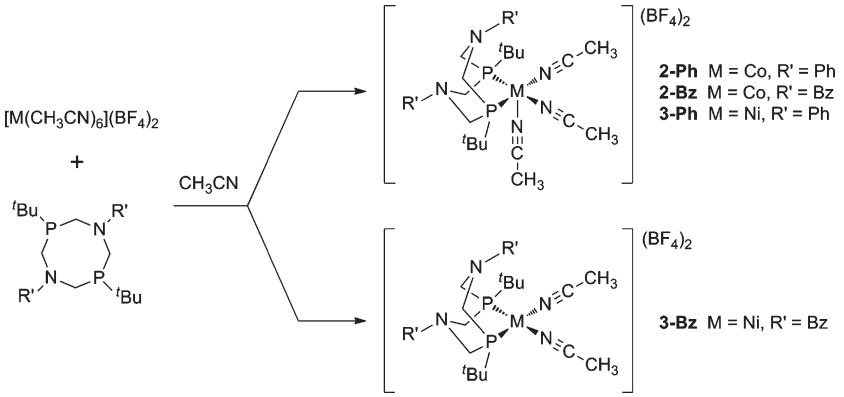

a 4:1 ratio (Figure S4, Supporting Information). The major conformer is assigned as a "crown" isomer on the basis of NMR data similar to that described above for crown-$P^{tBu}{}_2N^{Ph}{}_2$ (Figure S5, Supporting Information). For the minor conformer, two NCH_2Ph and three equal-intensity PCH_2N resonances are observed, while a fourth PCH_2N resonance appears to overlap with a resonance from the "crown" conformer, as determined by peak integration and a $^1H-^1H$ COSY spectrum (Figure S6, Supporting Information). The low symmetry indicated for this isomer is consistent with its assignment as a "chair-boat" conformer. Isomers with *tert*-butyl substituents on opposite faces of the eight-membered ring are less consistent with observed spectral data.

Synthesis and Characterization of Metal Complexes. The addition of 1 equiv of a cyclic $P^{tBu}{}_2N^{R'}{}_2$ ligand to an acetonitrile solution of $[Co(CH_3CN)_6](BF_4)_2$ or $[Ni(CH_3CN)_6](BF_4)_2$ followed by workup provides a convenient synthesis of $[Co(P^{tBu}{}_2N^{Ph}{}_2)(CH_3CN)_3](BF_4)_2$ (**2-Ph**), $[Co(P^{tBu}{}_2N^{Bz}{}_2)(CH_3CN)_3](BF_4)_2$ (**2-Bz**), $[Ni(P^{tBu}{}_2N^{Ph}{}_2)(CH_3CN)_3](BF_4)_2$ (**3-Ph**), and $[Ni(P^{tBu}{}_2N^{Bz}{}_2)(CH_3CN)_2](BF_4)_2$ (**3-Bz**) (Scheme 1). Elemental analyses of the products are consistent with these formulations. Magnetic moments of 1.81 and 1.95 μ_B were determined for **2-Ph** and **2-Bz**, respectively, using the Evans method. These value are consistent with low-spin Co(II) complexes with one unpaired spin.[24]

The nickel complexes were further characterized by NMR spectroscopy. The NMR spectra of $[Ni(P^{tBu}{}_2N^{Ph}{}_2)(CH_3CN)_3](BF_4)_2$ (**3-Ph**) show an interesting solvent dependence. In CD_2Cl_2, the room-temperature ^1H NMR spectrum displays sharp resonances consistent with a diamagnetic, five-coordinate, square-pyramidal complex. A single AB pattern is observed for the methylene protons of the ligand (4.26, 3.64 ppm), indicating that the two chelate rings of the ligand are equivalent or are rapidly interconverting. In the room-temperature $^{31}P\{^1H\}$ NMR spectrum in CD_2Cl_2, a broad singlet is observed at 11.9 ppm.

In contrast, the room-temperature ^1H NMR spectrum of **3-Ph** in CD_3CN displays a broad *tert*-butyl resonance at 3.5 ppm and a broad PCH_2N resonance at 8.1 ppm, both of which are shifted downfield from the typically observed ranges. The phenyl resonances are sharp and are in the normal range. When the solution is warmed to 80 °C, the *tert*-butyl and PCH_2N resonances sharpen and shift upfield to 2.5 and 6.3 ppm, respectively, and a second broad PCH_2N resonance is observed at 16.9 ppm (Figures S7 and S8, Supporting Information). Both PCH_2N resonances integrate to 4H relative to the *tert*-butyl group (18H), thus accounting for all of the methylene protons. In the $^{31}P\{^1H\}$ NMR spectrum at −40 °C in CD_3CN, a single broad resonance is observed for the diphosphine ligand at 9.6 ppm. However at room temperature and above, no phosphorus resonance is observed for this complex. These results suggest that in acetonitrile a paramagnetic contribution to the chemical shifts is occurring for **3-Ph**.

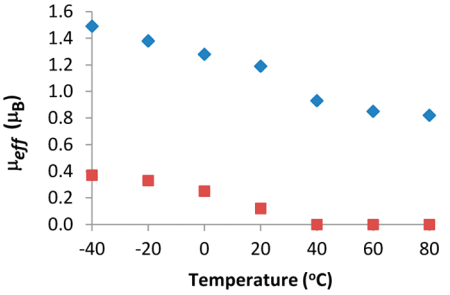

Figure 1. Plots of μ_{eff} as a function of temperature for $[Ni(P^{tBu}{}_2N^{Ph}{}_2)(CH_3CN)_3](BF_4)_2$ (**3-Ph**, blue trace) and $[Ni(P^{tBu}{}_2N^{Bz}{}_2)(CH_3CN)_2](BF_4)_2$ (**3-Bz**, red trace) in CD_3CN.

Determination of the solution magnetic moment (Evans method) for **3-Ph** in CD_3CN reveals an increase of μ_{eff} from 0.82 to 1.49 μ_B over the temperature range of +80 to −40 °C (Figure 1). These magnetic and NMR data are interpreted in terms of the equilibrium shown in Scheme 2, for which the square-pyramidal complex is diamagnetic and the six-coordinate complex is paramagnetic. Similar six-coordinate complexes with monodentate phosphine ligands have been proposed previously.[25] Increasing the temperature shifts the equilibrium to the left, which leads to an increase in the concentration of the diamagnetic five-coordinate species in solution and a decrease in the observed magnetic moment.

In contrast to the data for **3-Ph**, the room-temperature ^1H NMR spectrum of $[Ni(P^{tBu}{}_2N^{Bz}{}_2)(CH_3CN)_2](BF_4)_2$ (**3-Bz**) in CD_3CN displays resonances for the PCH_2N protons (4.37, 3.63 ppm) and the *tert*-butyl (1.29 ppm) groups within the

(24) (a) Attanasio, D. *Chem. Phys. Lett.* **1977**, *49*, 541–549. (b) Sethulakshmi, C. N.; Manoharan, P. T. *Inorg. Chem.* **1981**, *20*, 2533–2539. (c) Orlandini, A.; Sacconi, L. *Inorg. Chem.* **1976**, *15*, 78–85. (d) DuBois, D. L.; Miedaner, A. *Inorg. Chem.* **1986**, *25*, 4642–4650. (e) Pilloni, G.; Schiavon, G.; Zotti, G.; Zecchin, S. *J. Organomet. Chem.* **1977**, *134*, 305–318. (f) Bianchini, C.; Masi, D.; Mealli, C.; Sabat, M. *Gazz. Chim. Ital.* **1986**, *116*, 201–206. (g) Elian, M.; Hoffmann, R. *Inorg. Chem.* **1975**, *14*, 1058–1076.

(25) Bontempelli, G.; Magno, F.; Schiavon, G.; Corain, B. *Inorg. Chem.* **1981**, *20*, 2579–2590.

Scheme 2

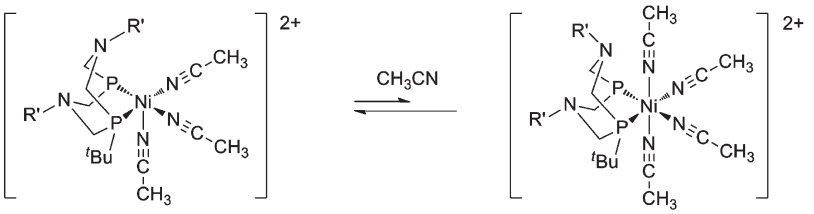

Scheme 3

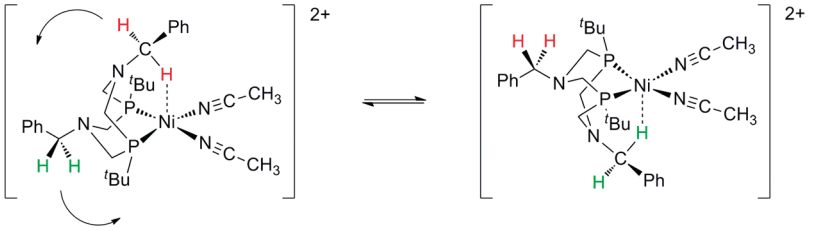

normal ranges expected for a diamagnetic complex. However, at room temperature the NCH_2Ph resonance appears as a broad hump in the baseline at ca. 5.7 ppm. When the solution is warmed to 80 °C, this resonance sharpens and shifts upfield to 5.0 ppm ($\Delta\nu_{1/2}$ ca. 72 Hz), while the remaining resonances remain unshifted (Figure S9, Supporting Information). Determination of the solution magnetic moment (Evans method) of **3-Bz** in CD_3CN results in small values for μ_{eff} at low temperatures (< 0.5 μ_B) and no observable paramagnetic character above 40 °C (Figure 1). As observed for **3-Ph**, a $^{31}P\{^1H\}$ NMR resonance for **3-Bz** is not observed at or above room temperature but does appear as a broad singlet at −2.5 ppm upon cooling the solution to −40 °C.

Complex **3-Bz** was not soluble in the weakly coordinating solvents THF, acetone, and CH_2Cl_2; however, it is soluble in CD_3NO_2. In the latter solvent at room temperature, the ^1H NMR resonances for **3-Bz** are broad but lie in the chemical shift range of a diamagnetic complex, and a broad $^{31}P\{^1H\}$ NMR resonance appears at 5.3 ppm. A single NCH_2Ph resonance that integrates to 4H is observed at 4.49 ppm at room temperature, and a singlet that integrates to 6H is also observed for the acetonitrile ligands at 2.42 ppm. When the sample is cooled to −20 °C, two equal-intensity NCH_2Ph resonances are observed at 5.08 and 3.91 ppm, with each resonance integrating to 2H (Figure S10, Supporting Information).

The NMR data for **3-Bz** in CD_3NO_2 are interpreted in terms of a weak agostic interaction of the methylene protons of the benzyl group with Ni, as shown in Scheme 3. At low temperature, one of the benzyl hydrogens interacts with nickel, resulting in a boat conformation for that ring system, while the other six-membered ring has a chair conformation. At room temperature the benzyl hydrogen atoms of these two ring systems interchange, resulting in a single resonance for these protons. A weak agostic interaction is consistent with the X-ray diffraction study of this complex, discussed below. The value of the C−H coupling constant would provide additional support for an agostic hydrogen. However, no signals were observed for either NCH_2Ph group in the ^1H-coupled ^{13}C NMR spectrum of **3-Bz** recorded at −20 °C; therefore, a value for $^1J_{CH}$ could not be measured for this complex.

Structural Studies. Vapor diffusion of Et_2O into an acetonitrile solution of $[Co(P^{tBu}{}_2N^{Ph}{}_2)(CH_3CN)_3](BF_4)_2$ (**2-Ph**) or $[Co(P^{tBu}{}_2N^{Bz}{}_2)(CH_3CN)_3](BF_4)_2$ (**2-Bz**) resulted in the formation of dark brown crystals that were suitable for an X-ray diffraction study. The crystals consist of discrete cations and BF_4^- anions. Drawings of the cations are shown in Figure 2, and selected bond lengths and angles are given in Tables 1 and 2, respectively. The structures are best described as square pyramids with acetonitrile ligands occupying the axial positions. These structures and the metric parameters of the cations are similar to those previously determined for $[Co(P^{Ph}{}_2N^{Ph}{}_2)(CH_3CN)_3](BF_4)_2$, and in Tables 1 and 2, the values for the latter complex are included for comparison.[22]

In the structure of **2-Ph**, the Co−N bond distance for the axial acetonitrile (2.08 Å) is significantly longer than those of the two basal acetonitrile ligands (1.94 and 1.96 Å). The small bite angle observed for the diphosphine ligand (83.60°) is typical for cyclic $P^R{}_2N^{R'}{}_2$ ligands coordinated to divalent first-row transition metals. The N(3)−Co−N(4) angle of 85.50° between the two basal acetonitrile ligands is smaller than that observed for the analogous $[Co(P^{Ph}{}_2N^{Ph}{}_2)(CH_3CN)_3]^{2+}$ cation (88.7°).[22] This acute angle in **2-Ph** is attributed to steric interactions between the *tert*-butyl groups on the diphosphine ligand and the two basal acetonitrile ligands. Consistent with this explanation, the C−N−Co angles of the basal acetonitrile ligands are less than 180° (164.40 and 174.35°) and bend away from the *tert*-butyl groups. The corresponding angles for $[Co(P^{Ph}{}_2N^{Ph}{}_2)(CH_3CN)_3]^{2+}$ are 172.66 and 173.73°. In addition, the dihedral angle between the plane defined by the two N atoms of the basal acetonitrile ligands and cobalt and the plane defined by the two phosphorus atoms and cobalt is 18.98° for **2-Ph**. The corresponding angle for $[Co(P^{Ph}{}_2N^{Ph}{}_2)(CH_3CN)_3]^{2+}$ is 16.09°. Similar distortions are observed for the cation of **2-Bz** as well. In short, a comparison of the metric data for **2-Ph** and **2-Bz** with that of $[Co(P^{Ph}{}_2N^{Ph}{}_2)(CH_3CN)_3]^{2+}$ suggests that steric interactions between the bulky *tert*-butyl groups and the basal acetonitrile ligands result in small but notable distortions to relieve these interactions.

An examination of the diphosphine ligand conformations in **2-Ph** and **2-Bz** shows that each six-membered chelate ring adjacent to the axial acetonitrile ligand adopts a chair

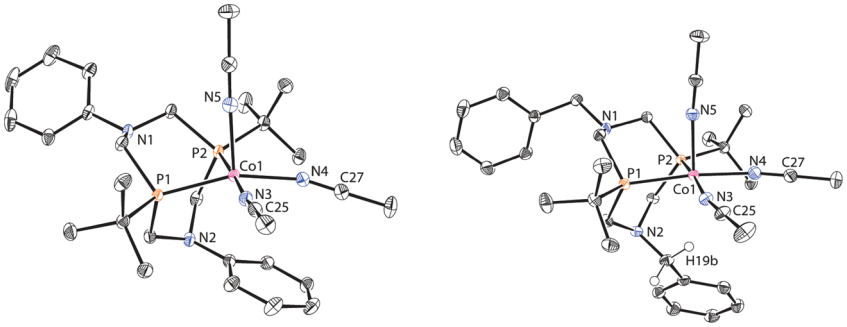

(a) $[Co(P^{tBu}{}_2N^{Ph}{}_2)(CH_3CN)_3]^{2+}$ (b) $[Co(P^{tBu}{}_2N^{Bz}{}_2)(CH_3CN)_3]^{2+}$

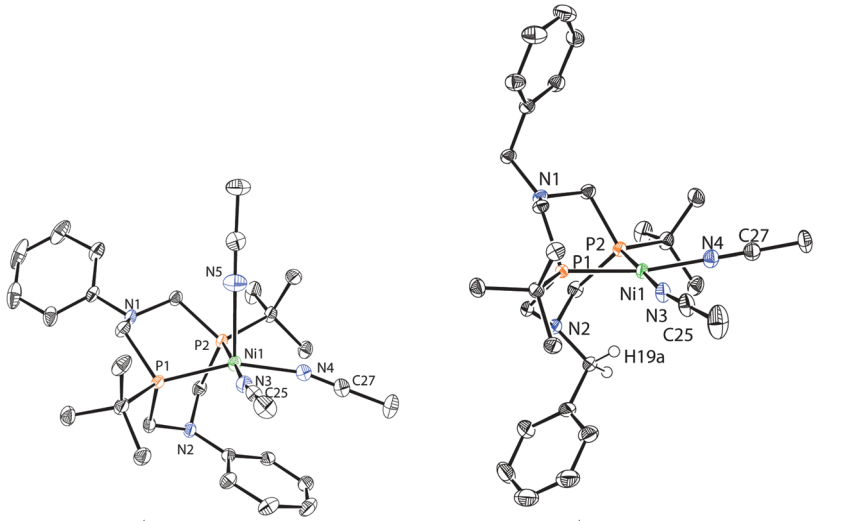

(c) $[Ni(P^{tBu}{}_2N^{Ph}{}_2)(CH_3CN)_3]^{2+}$ (d) $[Ni(P^{tBu}{}_2N^{Bz}{}_2)(CH_3CN)_2]^{2+}$

Figure 2. Drawings of molecular cations showing the atom-numbering scheme. The hydrogen atoms, except for those attached to the benzyl carbon of N(2), are omitted for clarity. Thermal ellipsoids are shown at the 50% probability level.

Table 1. Selected Bond Distances (Å)

compd	M−P(1)	M−P(2)	M−N(3)	M−N(4)	M−N(5)
$[Co(P^{Ph}{}_2N^{Ph}{}_2)(CH_3CN)_3]^{2+}$	2.1918(5)	2.1978(5)	1.9516(15)	1.9427(15)	2.0776(15)
$[Co(P^{tBu}{}_2N^{Ph}{}_2)(CH_3CN)_3]^{2+}$	2.2242(5)	2.2504(5)	1.9386(13)	1.9647(13)	2.0766(13)
$[Co(P^{tBu}{}_2N^{Bz}{}_2)(CH_3CN)_3]^{2+}$	2.2239(4)	2.2419(4)	1.9607(12)	1.9550(12)	2.0586(12)
$[Ni(P^{tBu}{}_2N^{Ph}{}_2)(CH_3CN)_3]^{2+}$	2.1881(6)	2.2158(6)	1.9141(18)	1.9451(17)	2.3113(18)
$[Ni(P^{tBu}{}_2N^{Bz}{}_2)(CH_3CN)_2]^{2+}$	2.1902(5)	2.1965(5)	1.9035(17)	1.9105(16)	

conformation to minimize steric interactions with acetonitrile, and the second six-membered ring of each ligand has a boat conformation. As a result the nonbonding Co···N(2) distances are 3.27 and 3.53 Å for **2-Ph** and **2-Bz**, respectively. Additionally, in **2-Ph** the N atom of the ring with the boat conformation is nearly planar and the attached phenyl ring folds over the cobalt atom, resulting in the close approach of the ipso (3.11 Å) and ortho (3.15 Å) carbon atoms to cobalt. For **2-Bz**, one of the hydrogen atoms on the benzyl attached to the N atom of the ring in the boat conformation is in close contact with the Co atom in this complex (2.76 Å). The paramagnetism of these complexes prevented the use of NMR spectral data to provide evidence for or against significant interactions between Co and either the C atoms of the phenyl rings or the H atoms of the benzyl carbons.

Red crystals of $[Ni(P^{tBu}{}_2N^{Ph}{}_2)(CH_3CN)_3](BF_4)_2$ (**3-Ph**) were grown by vapor diffusion of Et_2O into an acetonitrile solution of the complex. A drawing of the cation is shown in Figure 2, and selected bond lengths and angles are given in Tables 1 and 2, respectively. The structure of this nickel complex is very similar to that of the corresponding cobalt complex, **3-Ph**, with the most notable difference being the longer Ni−N(5) distance (2.31 Å) for the apical acetonitrile compared to that of the Co−N(5) distance (2.08 Å). This is consistent with the addition of a second electron into the d_{z^2} orbital that has antibonding character with respect to the σ orbital of the acetonitrile ligand. In addition, the Ni−C distances to the ipso (3.23 Å) and ortho (3.34 Å) carbon atoms of the phenyl ring folded over the Ni atom are slightly longer than the corresponding distances of **2-Ph**, 3.11 and 3.15 Å, respectively.

Red crystals of $[Ni(P^{tBu}{}_2N^{Bz}{}_2)(CH_3CN)_2](BF_4)_2$ (**3-Bz**) suitable for an X-ray diffraction study were grown by vapor diffusion of Et_2O into an acetonitrile solution of the complex. The crystal consists of discrete $[Ni(P^{tBu}{}_2N^{Bz}{}_2)(CH_3CN)_2]^{2+}$ cations and BF_4^- anions. A drawing of the cation is shown in Figure 2, and selected bond lengths and angles are given in Tables 1 and 2, respectively. The nickel is coordinated

Table 2. Selected Bond Angles (deg)

		$[Co(P^{Ph}{}_2N^{Ph}{}_2)(CH_3CN)_3]^{2+}$			
P(1)−Co(1)−P(2)	82.450(17)	P(2)−Co(1)−N(3)	172.61(4)	N(3)−Co(1)−N(5)	90.15(6)
P(1)−Co(1)−N(3)	95.08(4)	P(2)−Co(1)−N(4)	91.91(4)	N(4)−Co(1)−N(5)	96.53(6)
P(1)−Co(1)−N(4)	164.41(5)	P(2)−Co(1)−N(5)	97.09(4)	Co(1)−N(3)−C(25)	173.73(15)
P(1)−Co(1)−N(5)	98.58(4)	N(3)−Co(1)−N(4)	88.69(6)	Co(1)−N(4)−C(27)	172.65(15)
		$[Co(P^{tBu}{}_2N^{Ph}{}_2)(CH_3CN)_3]^{2+}$			
P(1)−Co(1)−P(2)	83.603(16)	P(2)−Co(1)−N(3)	177.67(4)	N(3)−Co(1)−N(5)	90.27(5)
P(1)−Co(1)−N(3)	94.08(4)	P(2)−Co(1)−N(4)	96.63(4)	N(4)−Co(1)−N(5)	98.12(5)
P(1)−Co(1)−N(4)	161.05(4)	P(2)−Co(1)−N(5)	90.38(4)	Co(1)−N(3)−C(25)	174.36(12)
P(1)−Co(1)−N(5)	100.82(4)	N(3)−Co(1)−N(4)	85.49(5)	Co(1)−N(4)−C(27)	164.40(11)
		$[Co(P^{tBu}{}_2N^{Bz}{}_2)(CH_3CN)_3]^{2+}$			
P(1)−Co(1)−P(2)	81.942(14)	P(2)−Co(1)−N(3)	170.96(4)	N(3)−Co(1)−N(5)	91.77(5)
P(1)−Co(1)−N(3)	97.61(4)	P(2)−Co(1)−N(4)	96.98(4)	N(4)−Co(1)−N(5)	90.34(5)
P(1)−Co(1)−N(4)	173.80(4)	P(2)−Co(1)−N(5)	97.26(4)	Co(1)−N(3)−C(25)	165.60(12)
P(1)−Co(1)−N(5)	95.85(3)	N(3)−Co(1)−N(4)	82.49(5)	Co(1)−N(4)−C(27)	167.31(12)
		$[Ni(P^{tBu}{}_2N^{Ph}{}_2)(CH_3CN)_3]^{2+}$			
P(1)−Ni(1)−P(2)	83.77(2)	P(2)−Ni(1)−N(3)	178.20(6)	N(3)−Ni(1)−N(5)	88.58(7)
P(1)−Ni(1)−N(3)	94.56(6)	P(2)−Ni(1)−N(4)	95.97(5)	N(4)−Ni(1)−N(5)	98.72(7)
P(1)−Ni(1)−N(4)	157.55(5)	P(2)−Ni(1)−N(5)	91.16(5)	Ni(1)−N(3)−C(25)	173.09(18)
P(1)−Ni(1)−N(5)	103.72(5)	N(3)−Ni(1)−N(4)	85.83(7)	Ni(1)−N(4)−C(27)	164.92(17)
		$[Ni(P^{tBu}{}_2N^{Bz}{}_2)(CH_3CN)_2]^{2+}$			
P(1)−Ni(1)−P(2)	83.489(18)	P(2)−Ni(1)−N(3)	178.84(5)	Ni(1)−N(3)−C(25)	164.68(17)
P(1)−Ni(1)−N(3)	96.50(5)	P(2)−Ni(1)−N(4)	96.54(5)	Ni(1)−N(4)−C(27)	163.55(16)
P(1)−Ni(1)−N(4)	169.67(5)	N(3)−Ni(1)−N(4)	83.69(7)		

to the diphosphine ligand and two acetonitrile ligands in a planar arrangement. The acute N(3)−Ni−N(4) angle of 83.6° and the bending of the two acetonitrile ligands away from the *tert*-butyl groups on phosphorus, as indicated by Ni−N−C angles of 163.5 and 164.8°, are again consistent with significant steric interactions between the two acetonitrile ligands and the *tert*-butyl groups on phosphorus. The diphosphine ligands adopt chair/boat conformations, and the N atom of the ring with a boat conformation is 3.49 Å from the Ni atom. One of the methylene hydrogen atoms on the benzyl group in the boat chelate is in close contact with the Ni atom in this complex (2.56 Å). This Ni···H distance is shorter than the sum of the van der Waals radii of Ni and H (2.72 Å),[26] suggesting that a weak agostic interaction is present. This Ni···H distance is also significantly shorter than the analogous Co···H distance in **2-Bz** (2.76 Å).

Electrochemical Studies. As shown in Figure 3, a cyclic voltammogram of $[Co(P^{tBu}{}_2N^{Ph}{}_2)_2(CH_3CN)_3](BF_4)_2$ (**2-Ph**) exhibits a single reversible reduction wave at $E_{1/2} = -0.87$ V ($\Delta E_p = 63$ mV) and a quasi-reversible oxidation wave at $E_{1/2} = +0.34$ V ($\Delta E_p = 114$ mV). A plot of the peak current (i_p) versus the square root of the scan rate for the wave at −0.87 V is linear, indicating that this is a diffusion-controlled process. This wave is assigned to the Co(II/I) couple. The quasi-reversible oxidation wave at +0.34 V is assigned to the Co(III/II) couple. Similar behavior is observed for **2-Bz**. For this complex the Co(II/I) couple is slightly more negative than that of the corresponding phenyl derivative, as expected, and the Co(III/II) couple is somewhat less reversible. Data for these complexes and related cobalt complexes are summarized in Table 3.

Figure 4 shows the cyclic voltammogram recorded on an acetonitrile solution of $[Ni(P^{tBu}{}_2N^{Ph}{}_2)(CH_3CN)_3](BF_4)_2$

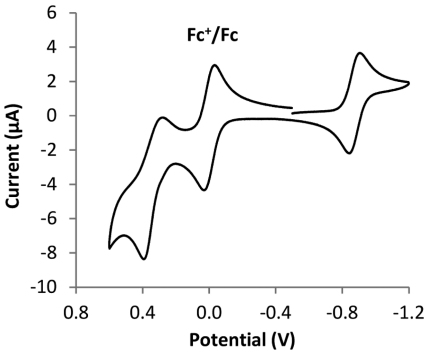

Figure 3. Cyclic voltammogram of a 2×10^{-3} M solution of $[Co(P^{tBu}{}_2N^{Ph}{}_2)(CH_3CN)_3](BF_4)_2$ (**2-Ph**). Conditions: scan rate 100 mV/s, 0.2 M NEt_4BF_4 (supporting electrolyte) acetonitrile solution, glassy-carbon working electrode. The wave at 0.0 V is the ferrocenium/ferrocene couple, used as an internal standard.

(**3-Ph**). Two reduction waves are observed for this complex at −0.59 and −1.61 V. The first reversible reduction wave is assigned to the Ni(II/I) couple. A plot of the peak current (i_p) versus the square root of the scan rate for the wave at −0.59 V is linear and indicates that this is a diffusion-controlled process. The second large reduction wave at −1.61 V is assigned to an irreversible Ni(I/0) couple. Similar results were obtained for $[Ni(P^{tBu}{}_2N^{Bz}{}_2)(CH_3CN)_2](BF_4)_2$ (**3-Bz**), and these results are summarized in Table 3.

A small reduction wave is observed consistently at −1.0 V in the cyclic voltammogram of **3-Ph**, and a small amount of free $P^{tBu}{}_2N^{Ph}{}_2$ (crown isomer) also is observed in the ^1H NMR spectrum of **3-Ph** in CD_3CN (but not in CD_2Cl_2). The relative intensity of the wave at −1.0 V is similar to the relative intensity of the ^1H NMR resonances observed for the free $P^{tBu}{}_2N^{Ph}{}_2$. Addition of $P^{tBu}{}_2N^{Ph}{}_2$ to acetonitrile solutions of **3-Ph** leads to an increase in the intensity of the wave

(26) (a) Bondi, A. *J. Phys. Chem.* **1964**, *68*, 441–452. (b) Rowland, R. S.; Taylor, R. *J. Phys. Chem.* **1996**, *100*, 7384–7391.

Table 3. Cyclic Voltammetry Parameters for Cobalt and Nickel Complexes

complex	$E_{1/2}$(III/II)[a] (ΔE_p)[b] [i_a/i_c][c]	$E_{1/2}$(II/I)[a] (ΔE_p)[b] [i_a/i_c][c]	E_p(I/0) (irr)[d], $E_{1/2}$(I/0)	ref
$[Co(P^{tBu}{}_2N^{Ph}{}_2)(CH_3CN)_3](BF_4)_2$	+0.34 (114) [0.4]	−0.87 (63) [1.0]		this work
$[Co(P^{tBu}{}_2N^{Bz}{}_2)(CH_3CN)_3](BF_4)_2$	+0.26 (161) [2.2]	−0.94 (82) [1.1]		this work
$[Co(P^{Ph}{}_2N^{Ph}{}_2)(CH_3CN)_3](BF_4)_2$		−0.99 (70) [1.0]		22
$[Co(dppp)(CH_3CN)_3](BF_4)_2$		−0.91 (72) [1.0]		22
$[Co(CH_3CN)_6](BF_4)_2$		−1.21 (95) [0.9]		22
$[Co(P^{Ph}{}_2N^{Ph}{}_2)_2(CH_3CN)](BF_4)_2$		−0.58 (71) [1.0]		22
$[Ni(P^{tBu}{}_2N^{Ph}{}_2)(CH_3CN)_2](BF_4)_2$		−0.59 (99) [1.1]	−1.61 (irr)	this work
$[Ni(P^{tBu}{}_2N^{Bz}{}_2)(CH_3CN)_2](BF_4)_2$		−0.69 (104) [1.0]	−1.82 (irr)	this work
$[Ni(P^{Ph}{}_2N^{Ph}{}_2)_2(CH_3CN)](BF_4)_2$		−0.84	−1.02	18
$[Ni(P^{Ph}{}_2N^{Bz}{}_2)_2(CH_3CN)](BF_4)_2$		−0.94	−1.19	20
$[Ni(P^{Cy}{}_2N^{Bz}{}_2)_2](BF_4)_2$		−0.80	−1.28	18

[a] Half-wave potential in volts versus the $FeCp_2{}^+/FeCp_2$ couple in 0.2 M NEt_4BF_4/CH_3CN solutions. [b] Separation of cathodic and anodic peak potentials at a scan rate of 100 mV/s. Under these conditions ferrocene exhibited ΔE_p values of 70 ± 5 mV. [c] Ratio of anodic and cathodic peak currents at 100 mV/s. [d] Peak potential of irreversible Ni(I/0) couple.

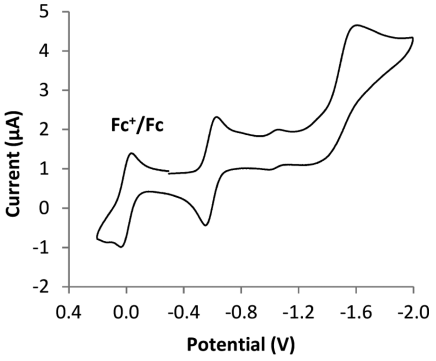

Figure 4. Cyclic voltammogram of a 2×10^{-3} M solution of $[Ni(P^{tBu}{}_2N^{Ph}{}_2)(CH_3CN)_3](BF_4)_2$ (**3-Ph**). Conditions: scan rate 100 mV/s, 0.2 M NEt_4BF_4 (supporting electrolyte) acetonitrile solution, glassy-carbon working electrode. The wave at 0.0 V is the ferrocenium/ferrocene couple used as an internal standard.

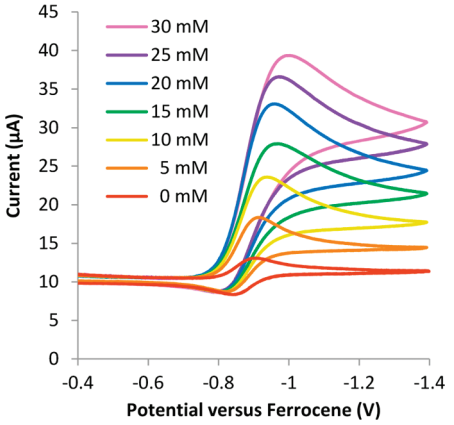

Figure 5. Successive cyclic voltammograms of a 0.002 M solution of $[Co(P^{tBu}{}_2N^{Ph}{}_2)(CH_3CN)_3](BF_4)_2$ in acetonitrile at increasing concentrations of 4-bromoanilinium tetrafluoroborate. Conditions: scan rate 50 mV/s, 0.2 M NEt_4BF_4 (supporting electrolyte), glassy-carbon working electrode. Potentials are referenced to the ferrocenium/ferrocene couple at 0.0 V (not shown).

at −1.0 V, while the intensity of the Ni(II/I) couple of **3-Ph** remains unchanged. The free ligand $P^{tBu}{}_2N^{Ph}{}_2$ does not give an electrochemical response in this potential range, and so the wave at −1.0 V is attributed to the reduction of $[Ni^I(P^{tBu}{}_2N^{Ph}{}_2)_2(CH_3CN)](BF_4)$ formed from the reaction of the free ligand with electrochemically generated $[Ni^I(P^{tBu}{}_2N^{Ph}{}_2)(CH_3CN)_n](BF_4)$. Further studies of this bis(diphosphine) Ni complex are in progress. Spontaneous ligand dissociation and rearrangement are not observed for **3-Bz** on the CV time scale.

Catalytic Hydrogen Production. Figure 5 shows successive cyclic voltammograms of $[Co(P^{tBu}{}_2N^{Ph}{}_2)(CH_3CN)_3](BF_4)_2$ (**2-Ph**) recorded in acetonitrile with increasing concentrations of 4-bromoanilinium tetrafluoroborate as the acid (pK_a = 9.43).[27] The cyclic voltammogram of **2-Ph** exhibits a catalytic wave for the reduction of protons at a half-wave potential of −0.88 V in the presence of 0.03 M acid. This potential agrees well with the Co(II/I) potential of the catalyst and corresponds to an overpotential of approximately 160 mV using the method proposed by Evans et al. for determining overpotentials.[28]

The top two graphs in Figure 6 show plots of i_{cat}/i_p (where i_{cat} is the peak current in the presence of acid and i_p is the peak current in the absence of acid) versus acid concentration. The linear region of this plot at low acid concentrations (top graph) is consistent with a second-order dependence of the overall catalytic rate on acid.[29,30] At higher concentrations of acid (middle graph), no acid dependence is observed, and this is tentatively interpreted in terms of a rate-limiting elimination of H_2 under these conditions. Using the limiting current in this acid-independent region, a turnover frequency of 160 s^{-1} can be calculated for **2-Ph** using eq 1.[29,30] A linear relationship is observed between i_{cat} and [**2-Ph**], which demonstrates a first-order dependence of the catalytic current on the concentration of catalyst at constant acid concentration (0.1 M, bottom graph in Figure 6) using eq 2.[29,30] A controlled-potential electrolysis experiment was performed on the complex at −1.11 V in the presence of 4-bromoanilinium tetrafluoroborate, and the evolution of H_2 was confirmed by gas chromatography (current efficiency 96 ± 5%).

$$\frac{i_{cat}}{i_p} = \frac{2}{0.446}\sqrt{\frac{RTk}{Fv}} \qquad (1)$$

$$i_{cat} = nFA[\mathrm{Cat}]_T(Dk)^{1/2} \qquad (2)$$

(27) Kaljurand, I.; Kutt, A.; Soovali, L.; Rodima, T.; Maemets, V.; Leito, I.; Koppel, I. A. *J. Org. Chem.* **2005**, *70*, 1019–1028.
(28) Felton, G. A. N.; Glass, R. S.; Lichtenberger, D. L.; Evans, D. H. *Inorg. Chem.* **2006**, *45*, 9181–9184.
(29) Pool, D.; DuBois, D. L. *J. Organomet. Chem.* **2009**, *694*, 2858–2865.
(30) (a) Delehay, P.; Stiehl, G. L. *J. Am. Chem. Soc.* **1952**, *74*, 3500–3505. (b) Nicholson, R. S.; Shain, I. *Anal. Chem.* **1964**, *36*, 706–723. (c) Saveant, J. M.; Vianello, E. *Electrochim. Acta* **1965**, *10*, 905–920. (d) Saveant, J. M.; Vianello, E. *Electrochim. Acta* **1967**, *12*, 629–646.

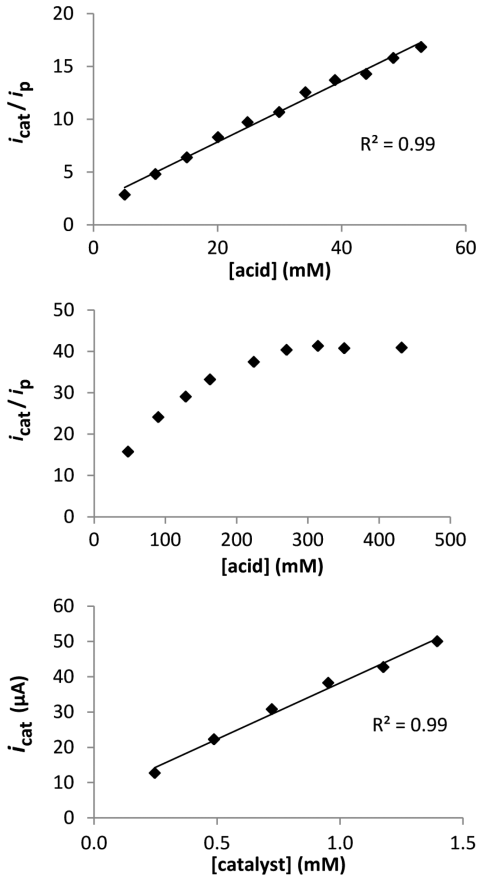

Figure 6. Plots of the i_{cat}/i_p ratio as a function of the concentration of 4-bromoanilinium tetrafluoroborate added to a 0.002−0.001 M acetonitrile solution of $[Co(P^{tBu}{}_2N^{Ph}{}_2)(CH_3CN)_3](BF_4)_2$ (top and middle graphs) and a plot of catalytic current vs concentration of $[Co(P^{tBu}{}_2N^{Ph}{}_2)(CH_3CN)_3](BF_4)_2$ in an acetonitrile solution containing 0.1 M 4-bromoanilinium tetrafluoroborate (bottom graph). Conditions: scan rate 50 mV/s, 0.2 M NEt_4BF_4 (supporting electrolyte) acetonitrile solution, glassy-carbon working electrode.

Similar studies were attempted with **2-Ph** using 4-cyanoanilinium tetrafluoroborate (pK_a = 7.0 in acetonitrile)[31] (Figure S11, Supporting Information) and 2,6-dichloroanilinium tetrafluoroborate (pK_a = 5.1 in acetonitrile)[27] (Figure S12, Supporting Information) as acids. Catalytic currents for each of these acids were observed to be higher than those with 4-bromoanilinium tetrafluoroborate. However, a negative shift in both the catalytic onset potential and half-peak potential was observed as the acid concentration was increased. The half-peak potential reached a maximum of −1.1 V for 4-cyanoanilinium tetrafluoroborate and −1.3 V for 2,6-dichloroanilinium tetrafluoroborate (Figure 7). Both of these potentials are near the half-wave potential of $[Co(CH_3CN)_6]^{2+}$ at −1.21 V. In contrast, when using 4-bromoanilinium tetrafluoroborate at similar acid concentrations the observed half-peak potential reaches a maximum of −0.92 V, which is close to the half-wave potential of −0.87 V for **2-Ph**.

The UV−vis spectra of 0.001 M acetonitrile solutions of **2-Ph** in the presence of 0.075 M solutions of each acid were monitored with time in order to determine the relative stability of **2-Ph** (Figure S13, Supporting Information).

(31) Appel, A. M.; Lee, S.-J.; Franz, J. A.; DuBois, D. L.; Rakowski DuBois, M.; Twamley, B. *Organometallics* **2009**, *28*, 749–754.

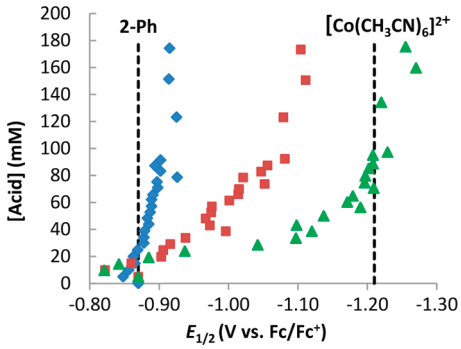

Figure 7. Plot of $E_{1/2}$ of the catalytic wave as a function of the concentration of 4-bromoanilinium tetrafluoroborate (blue trace), 4-cyanoanilinium tetrafluoroborate (red trace), and 2,6-dichloroanilinium tetrafluoroborate (green trace) for a 0.002 M acetonitrile solution of $[Co(P^{tBu}{}_2N^{Ph}{}_2)(CH_3CN)_3](BF_4)_2$ (**2-Ph**). The vertical lines at −0.84 and −1.21 V represent the $E_{1/2}$ values for **2-Ph** and $[Co(CH_3CN)_6]^{2+}$, respectively. Conditions: scan rate 50 mV/s, 0.2 M NEt_4BF_4 (supporting electrolyte) acetonitrile solution, glassy-carbon working electrode.

For a 75:1 ratio of acid to **2-Ph**, the complex decomposes to form $[Co(CH_3CN)_6]^{2+}$ with a half-life of approximately 40 min for 4-cyanoanilinium tetrafluoroborate and 18 min for 2,6-dichloroanilinium tetrafluoroborate. In contrast, **2-Ph** displays a half-life of 190 min in the presence of 4-bromoanilinium tetrafluoroborate. These data indicate that **2-Ph** is significantly less stable in the presence of 4-cyanoanilinium or 2,6-dichloroanilinium salts; therefore, $[Co(CH_3CN)_6]^{2+}$ likely contributes significantly to the observed catalytic currents. As a result, meaningful comparisons of catalytic currents using these acids with those for 4-bromoanilinium tetrafluoroborate are not possible.

The complex $[Co(P^{tBu}{}_2N^{Bz}{}_2)(CH_3CN)_3](BF_4)_2$ (**2-Bz**) has more basic N atoms than **2-Ph** because the benzyl substituents are more electron-donating than phenyl groups. When **2-Bz** is treated with small quantities of 4-bromoanilinium tetrafluoroborate (0.005 M), the Co(II/I) half-wave potential shifts from −0.94 to −0.79 V, presumably as a result of protonation of a benzyl amine (Figure S17, Supporting Information). Additionally, a new irreversible reduction wave appears at a half-wave potential of −1.08 V. At 0.030 M of 4-bromoanilinium tetrafluoroborate (a moderate acid concentration for catalytic studies) the half-wave potential of the catalytic wave has shifted to −1.29 V, suggesting that the proton reduction is associated with $[Co(CH_3CN)_6]^{2+}$ formed through loss of the protonated $P^{tBu}{}_2N^{Bz}{}_2$ ligand. The decomposition is even more rapid when using 4-cyanoanilinium tetrafluoroborate.

The nickel complexes **3-Ph** and **3-Bz** were also investigated for electrocatalytic proton reduction, but no catalytic activity was observed at the Ni(II/I) couple for either complex (Figure S18 and S19, Supporting Information). The complex **3-Ph** shows some degradation in the presence of small amounts of 4-cyanoanilinium tetrafluoroborate (25 mM), while **3-Bz** decomposes much more quickly (within 15 min) at similar concentrations of the same acid. When 2,6-dichloroanilinium tetrafluoroborate is used, **3-Ph** also decomposes by ca. 60% within 35 min. Therefore, the $[Ni(P^{tBu}{}_2N^{R'}{}_2)(CH_3CN)_n](BF_4)_2$ (n = 2, 3) complexes show acid stability similar to that of $[Co(P^{tBu}{}_2N^{R'}{}_2)(CH_3CN)_3](BF_4)_2$ while displaying no catalytic activity at modest potentials.

Discussion

Complex Characterization. The cyclic $P^R{}_2N^{R'}{}_2$ ligands with *tert*-butyl substituents on phosphorus favor the formation of mono(diphosphine) complexes with both cobalt and nickel. Five-coordinate, square-pyramidal products of the formula $[M(P^{tBu}{}_2N^{R'}{}_2)(CH_3CN)_3]^{2+}$ (**2-Ph**, **2-Bz**, and **3-Ph**) and the agostic complex $[Ni(P^{tBu}{}_2N^{Bz}{}_2)(CH_3CN)_2]^{2+}$ (**3-Bz**) have been isolated and characterized. The formation of mononuclear bis(diphosphine) complexes of the type $[M(P^{tBu}{}_2N^{R'}{}_2)_2]^{2+}$ was not observed under conditions studied here, even for nickel, for which the quite sterically hindered analogue with cyclohexylphosphine donors has been prepared previously.[18] Further evidence of the steric demands of these ligands was observed in the X-ray diffraction studies of the products. Complexes **2-Ph**, **2-Bz**, **3-Ph**, and **3-Bz** all display small N−M−N angles in the range of 82−85°, and one or both of the basal acetonitrile ligands are bent away from the bulky phosphine substituents with M−N−C angles of 163−165°. The basal planes of the molecules show small tetrahedral distortions with dihedral angles of ca. 18° between the P−M−P and N−M−N planes. These structural distortions have a marked effect on the reduction potentials of the complexes, which are discussed below.

For the cobalt complexes **2-Ph** and **2-Bz**, the structures observed in the solid state are likely preserved in solution with the exception of ring conformations. The solution magnetic moments of 1.8−1.95 μ_B are consistent with low-spin square-pyramidal complexes. Similarly, the crystal structure of $[Ni(P^{tBu}{}_2N^{Ph}{}_2)(CH_3CN)_3](BF_4)_2$ (**3-Ph**) reveals a square-pyramidal geometry that appears to be preserved in noncoordinating solvents such as dichloromethane. However, the variable-temperature NMR and magnetic susceptibility studies indicate that an equilibrium involving coordination of a solvent molecule occurs in acetonitrile solution to form a paramagnetic six-coordinate complex containing the diphosphine ligand and four acetonitrile ligands. The six-coordinate complex is present in the greatest quantity at low temperatures but persists at elevated temperatures. This six-coordinate formulation is similar to that proposed previously for $[Ni(PPh_3)_2(CH_3CN)_4]^{2+}$.[25]

The structure of $[Ni(P^{tBu}{}_2N^{Bz}{}_2)(CH_3CN)_2](BF_4)_2$ (**3-Bz**) is unique in this series. The data confirm that only two acetonitrile ligands are present, both in the basal plane. The fifth coordination site of the square-pyramidal structure is occupied by a methylene hydrogen from the benzyl substituent of a ligand chelate ring in the boat conformation. The structure provides evidence for a weak agostic interaction with a H···Ni distance of 2.56 Å, significantly shorter than the sum of the van der Waals radii of these atoms of 2.72 Å. The fluxional nature of this weak agostic interaction, as shown in Scheme 3, is supported by variable-temperature NMR studies in both CD_3NO_2 and CD_3CN. A lower magnetic moment is observed for **3-Bz** compared to **3-Ph** (Figure 1), and this is attributed to the suppression of axial acetonitrile coordination by the agostic interaction in **3-Bz**.

Relationships Between Structure and Redox Potentials. Comparison of the Co(II/I) potentials for $[Co(P^{tBu}{}_2N^{Ph}{}_2)(CH_3CN)_3](BF_4)_2$ (**2-Ph**) and $[Co(P^{Ph}{}_2N^{Ph}{}_2)(CH_3CN)_3](BF_4)_2$ indicates that replacing a phenyl with a *tert*-butyl group on phosphorus results in a positive shift in the potential of this couple by 0.12 V. The positive shift is surprising because *tert*-butyl groups are expected to be significantly better electron donors than phenyl substituents. This shift is attributed to the steric interactions between the *tert*-butyl groups and the acetonitrile ligands, discussed above, that result in a distortion from the square-planar geometry in the basal plane of the structure. The antibonding overlaps of the basal ligands with the d_{z^2} orbital are reduced as a result of this distortion leading to more positive redox potentials.[32] A similar positive shift in potential has been observed for the Ni(II/I) couple of $[Ni(P^{Cy}{}_2N^{Bz}{}_2)_2](BF_4)_2$ relative to that of $[Ni(P^{Ph}{}_2N^{Bz}{}_2)_2(CH_3CN)](BF_4)_2$, as shown in the last two entries of Table 3. The bulky cyclohexyl substituents on phosphorus also result in distortions from a square-planar structure and a resulting stabilization of the LUMO.[20]

A second interesting feature of the electrochemical data is that replacement of a diphosphine ligand with acetonitrile ligands results in the redox potentials of the Co(II/I) couple becoming more negative: i.e., $[Co(P^{Ph}{}_2N^{Ph}{}_2)_2(CH_3CN)](BF_4)_2$ (−0.58 V), $[Co(P^{Ph}{}_2N^{Ph}{}_2)(CH_3CN)_3](BF_4)_2$ (−0.99 V), and $[Co(CH_3CN)_6](BF_4)_2$ (−1.21 V). However, opposing trends are observed for the nickel complexes. For the last five entries in Table 3, replacing phosphine ligands with acetonitrile ligands result in positive potential shifts for the Ni(II/I) couple but negative shifts for the potentials of the Ni(I/0) couples. The origin of these differences between cobalt and nickel is not clear. It can also be seen from Table 3 that replacement of phenyl substituents on nitrogen with benzyl substituents results in a shift of the M(II/I) couple to more negative potentials by 0.07−0.10 V. This observation is also true for Ni(II/I) couples previously reported for $[Ni(P^{Ph}{}_2N^{Ph}{}_2)_2(CH_3CN)]^{2+}$ (−0.84 V) and $[Ni(P^{Ph}{}_2N^{Bz}{}_2)_2(CH_3CN)]^{2+}$ (−0.94 V).[20] The potential shifts that are observed as a result of changing substituents on nitrogen indicate that there is effective electronic communication between the pendant base of these $P^R{}_2N^{R'}{}_2$ ligands and the metal.

Comparisons of Catalytic Properties. Our results indicate that $[Co(P^{tBu}{}_2N^{Ph}{}_2)(CH_3CN)_3](BF_4)_2$ (**2-Ph**) is an effective catalyst for the electrochemical reduction of protons to H_2 using 4-bromoanilinium tetrafluoroborate as the acid, with the onset of the catalytic current occurring at the Co(II/I) couple. Kinetic studies of the catalytic reaction are consistent with pre-equilibrium steps involving the addition of two protons to a Co(I) complex, followed by a rate-determining step that is first order in catalyst. This rate-determining step could involve either H_2 elimination or an intramolecular proton transfer step. Similar kinetic behavior has been observed previously for $[Ni(P^{Ph}{}_2N^{R'}{}_2)_2(CH_3CN)](BF_4)_2$ complexes[18,19] and for $[Co(P^{Ph}{}_2N^{Ph}{}_2)(CH_3CN)_3](BF_4)_2$.[22] In those studies, H_2 loss was favored as the rate-determining step, because in most cases where we have been able to observe it spectroscopically, intramolecular proton transfer for complexes containing $P^R{}_2N^{R'}{}_2$ ligands has been fast.

As discussed above, the substitution of the *tert*-butyl substituent for phenyl on the cyclic phosphine ligand in these cobalt derivatives results in a positive shift of the Co(II/I) couple observed for **2-Ph**, and this change in potential is consistent with our observations of a reduction of the overpotential (160 mV for **2-Ph** vs 285 mV for $[Co(P^{Ph}{}_2N^{Ph}{}_2)(CH_3CN)_3](BF_4)_2$ when 4-bromoanilinium tetrafluoroborate is the acid). The reduction in overpotential for **2-Ph** is accompanied by a small increase in rate (160 s^{-1} for **2-Ph** vs

(32) (a) Nimlos, M. R.; Chang, C. H.; Curtis, C. J.; Miedaner, A.; Pilath, H. M.; DuBois, D. L. *Organometallics* **2008**, *27*, 2715–2722. (b) Miedaner, A.; Haltiwanger, R. C.; DuBois, D. L. *Inorg. Chem.* **1991**, *30*, 417–427.

90 s^{-1} for $[Co(P^{Ph}_2N^{Ph}_2)(CH_3CN)_3](BF_4)_2$. The catalytic rates and overpotentials for **2-Ph** are quite comparable to those of several $[Ni(P^{Ph}_2N^{R'}_2)_2(CH_3CN)](BF_4)_2$ catalysts reported previously by our group. For example, $[Ni(P^{Ph}_2N^{R'}_2)_2(CH_3CN)](BF_4)_2$ (where R′ = (thiophene-3-yl)phenyl) has a turnover frequency of 56 s^{-1} and an estimated overpotential of 280 mV under similar conditions.[29]

In contrast to **2-Ph**, the corresponding benzyl derivative **2-Bz** is not an effective catalyst for H_2 production. In this case protonation of the more basic amine in the ligand occurs before reduction of the complex to Co(I), and this protonation results in rapid loss of ligand. Similar decomposition of the catalyst **2-Ph** is also observed when stronger acids such as 2,6-dichloroanilinium tetrafluoroborate are used. Our earlier observation that $[Co(P^{Ph}_2N^{Ph}_2)(CH_3CN)_3](BF_4)_2$ is an effective catalyst even in the presence of triflic acid suggests that the introduction of the *tert*-butyl substituent significantly reduces the overall stabilities of the complexes toward acid. The nickel complexes **3-Ph** and **3-Bz** were also found to be ineffective as catalysts for hydrogen formation. The relatively positive potentials observed for the Ni(II/I) couples in these complexes (see Table 3) require that somewhat stronger acids be used than in the cobalt systems, and under these conditions complex decomposition, via ligand protonation and dissociation, is relatively rapid. Again we note that previously studied $[Ni(P^{Ph}_2N^{R'}_2)_2]^{2+}$ derivatives were significantly more stable in the presence of acid. Nevertheless, no evidence for a catalytic wave for hydrogen formation was observed in our studies of **3-Ph** and **3-Bz**, even at low acid concentrations when the complexes are still intact. The lack of activity is consistent with our earlier observations that two positioned bases appear to be important for the catalytic activity of nickel diphosphine complexes.[21]

In summary, our results indicate that cobalt complexes containing a single diphosphine ligand with a positioned pendant base constitute a promising class of catalysts for further study and optimization. The comparative studies reported here are relevant to further catalyst optimization, because they demonstrate that the variation of either the phosphorus or nitrogen substituent in the cyclic $P^{R}_2N^{R'}_2$ ligands can result in significant consequences for the metal complex stoichiometry, structure, redox properties, and catalytic activity.

Experimental Section

General Experimental Procedures. ^1H and $^{31}P\{^1H\}$ NMR spectra were recorded on a Varian Inova spectrometer (500 MHz for ^1H) at 20 °C unless otherwise noted. All ^1H chemical shifts have been internally calibrated to the monoprotio impurity of the deuterated solvent. The $^{31}P\{^1H\}$ NMR spectra were referenced to external phosphoric acid at 0 ppm. Magnetic moments were determined by the Evans method[33] in CD_3CN solution containing $SiMe_4$. UV−vis spectra were recorded on a Shimadzu UV-2401 PC spectrometer using UV Probe (version 1.10) software. MM2 calculations were performed using the software embedded within ChemBio3D Ultra, version 12.0. Gas chromatograms were recorded on an Agilent Technologies 6850 Networks GC system equipped with an Agilent HP-1 column (30 m length × 0.530 mm i.d. × 2.65 μm film) and a thermal conductivity detector using argon as the carrier gas.

Electrochemical measurements were performed using a CH Instruments 660C potentiostat equipped with a standard three-electrode cell consisting of an oven-dried 4−5 mL conical vial fitted with a polysilicone cap having openings sized to closely accept each electrode. For each experiment, the cell was assembled and used under a flow of nitrogen that was bubbled through dry acetonitrile. Immediately prior to each measurement, the working electrode (1 mm PEEK-encased glassy carbon, Cypress Systems EE040) was polished using grade 3 alumina polishing gamal (Fisher A446-100) and then rinsed with neat acetonitrile. A glassy-carbon rod (Structure Probe, Inc.) was used as the counterelectrode, and a silver wire suspended in a solution of Et_4NBF_4 (0.2 M) in acetonitrile and separated from the analyte solution by a Vycor frit (CH Instruments 112) was used as a pseudo reference electrode. Ferrocene was used as an internal standard, and all potentials are referenced to the ferrocenium/ferrocene couple at 0 V.

Methods and Materials. All manipulations were carried out under N_2 using standard vacuum line, Schlenk, and inert-atmosphere glovebox techniques. Solvents were purified by passage through neutral alumina using an Innovative Technology, Inc., Pure Solv solvent purification system. NMR solvents were purchased from Cambridge Isotope and were dried, degassed, and distilled prior to use. Tetraethylammonium tetrafluoroborate was dried in vacuo at room temperature for 2 days. Anilinium salts were prepared by reaction of the parent aniline with 1.5 equiv of $HBF_4 \cdot Et_2O$, and then the crude salts were recrystallized from CH_3CN/Et_2O. *tert*-Butylphosphine was purchased from Strem Chemicals. $[Co(CH_3CN)_6](BF_4)_2$ and $[Ni(CH_3CN)_6](BF_4)_2$ were prepared according to literature procedures.[34]

Syntheses. $\mathbf{P^{tBu}_2N^{Ph}_2}$**.** *tert*-Butyl phosphine (2.0 mL, 0.016 mol, 1.0 equiv) was measured into a two-neck 100 mL round-bottom flask, which was then fitted with a rubber septum and a gas adapter. Degassed absolute EtOH (ca. 50 mL) was transferred by cannula into the flask, and then solid paraformaldehyde (1.07 g, 0.036 mol, 2.3 equiv) was added. The reaction mixture was stirred in an oil bath at 65 °C for 16 h, resulting in a clear solution. The solution was cooled to room temperature, and then aniline (1.5 mL, 0.016 mol, 1.0 equiv) was added via syringe over 10 min. The reaction mixture was heated in an oil bath at 65 °C for 23 h, causing a white precipitate to form. When the mixture was lowered to room temperature, the volatiles were removed in vacuo. The crude solid was slurried in CH_3CN (25 mL), and then the white powder was collected by vacuum filtration and rinsed with CH_3CN (25 mL) and CH_2Cl_2 (5 × 10 mL). Upon drying in vacuo, $P^{tBu}_2N^{Ph}_2$ (2.13 g, 0.005 mol, 63%) was obtained as a white powder. The product displayed a low solubility in both polar and nonpolar solvents. NMR analysis indicated the presence of two isomers in ca. a 1:1 ratio in solution, with the observed ratio varying for different samples. ^1H NMR integrations were determined individually for each isomer. *Crown isomer*: ^1H NMR (acetone-d_6) δ 7.09 (t, 4H, $^3J_{HH}$ = 8.1 Hz, Ar *H*), 6.71 (d, 4H, $^3J_{HH}$ = 8.1 Hz, Ar *H*), 6.52 (t, 2H, $^3J_{HH}$ = 8.1 Hz, Ar *H*), 4.35 (t, 4H, $^2J_{HH}$ = $^2J_{HP}$ = 14.8 Hz, $PCH_{eq}H_{ax}N$), 3.95 (dd, 4H, $^2J_{HH}$ = 14.8 Hz, $^2J_{HP}$ = 5.4 Hz, $PCH_{eq}H_{ax}N$), 1.28 (d, 18H, $^3J_{HP}$ = 9.4 Hz, $C(CH_3)_3$); $^{31}P\{^1H\}$ NMR (acetone-d_6) δ −27.8 (s). *Saddle isomer*: ^1H NMR (acetone-d_6) δ 7.14 (t, 4H, $^3J_{HH}$ = 8.1 Hz, Ar *H*), 6.97 (d, 4H, $^3J_{HH}$ = 8.1 Hz, Ar *H*), 6.63 (t, 2H, $^3J_{HH}$ = 6.7 Hz, Ar *H*), 4.08 (dd, 4H, $^2J_{HH}$ = 13.7 Hz, $^2J_{HP}$ = 4.7 Hz, $PCH_{eq}H_{ax}N$), 3.71 (t, 4H, $^2J_{HH}$ = $^2J_{HP}$ = 14.8 Hz, $PCH_{eq}H_{ax}N$), 1.23 (d, 18H, d, 18H, $^3J_{HP}$ = 10.8 Hz, $C(CH_3)_3$); $^{31}P\{^1H\}$ NMR (acetone-d_6) δ −18.24. Anal. Calcd for $C_{24}H_{36}N_2P_2$: C, 69.54; H, 8.75; N, 6.76. Found: C, 69.36; H, 8.80; N, 6.71.

$\mathbf{P^{tBu}_2N^{Bz}_2}$**.** *tert*-Butyl phosphine (5.6 g, 0.062 mol), paraformaldehyde (3.73 g, 0.124 mol), and ethanol (100 mL) were combined in a Schlenk flask and heated to 60 °C for 12 h.

(33) (a) Evans, D. F. *J. Chem. Soc.* **1959**, 2003–2005. (b) Schubert, E. M. *J. Chem. Educ.* **1992**, *69*, 62. (c) Baker, M. V.; Field, L. D.; Hambley, T. W. *Inorg. Chem.* **1988**, *27*, 2872–2876.

(34) (a) Heintz, R. A.; Smith, J. A.; Szalay, P. S.; Weisgerber, A.; Dunbar, K. R.; Beck, K.; Coucouvanis, D. *Inorg. Synth.* **2002**, *33*, 75–83. (b) Hathaway, B. J.; Holah, D. E.; Underhill, A. E. *J. Chem. Soc.* **1962**, 2444–2448.

Benzylamine (6.66 g, 0.062 mol) was then added to the solution dropwise, and the reaction was maintained at 60 °C for another 12 h. The solution was cooled to room temperature, and the solvent was reduced to about 20 mL under reduced pressure and then filtered to isolate the insoluble product. The white precipitate was washed with 3 × 15 mL of ethanol to give 13 g of $P^{tBu}{}_2N^{Bz}{}_2$ (95% yield). ^{1}H NMR (acetone-d_6): δ 7.39 (d, 4H, $^3J_{HH}$ = 7.0 Hz, Ar *H*), 7.31 (t, 4H, $^3J_{HH}$ = 7.4 Hz, Ar *H*), 7.22 (t, 2H, $^3J_{HH}$ = 7.3 Hz, Ar *H*), 3.99 (s, 4H, NCH_2Ph), 3.20 (s, 8H, PCH_2N), 0.78 (s, 18H, C(CH_3)$_3$). ^{31}P{^{1}H} NMR (acetone-d_6): −45.1 (br s). ^{1}H NMR (THF-d_8, −50 °C): δ 7.45−7.10 (12.2H, Ar *H*, crown + chair-boat), 4.07 (s, 4.0H, NCH$_2$Ph, crown), 3.92 (s, 0.5H, NCH$_2$Ph, chair-boat), 3.72 (s, 0.5H, NCH$_2$Ph, chair-boat), 3.46 (d, 4.5H, $^2J_{HH}$ = 14.3 Hz, PCH_2N, crown + chair-boat), 3.20 (d, 4.0H, $^2J_{HH}$ = 14.4 Hz, PCH_2N, crown), 2.87 (d, 0.5H, $^2J_{HH}$ = 11.8 Hz, PCH_2N, chair-boat), 2.80 (d, 0.5H, $^2J_{HH}$ = 13.9 Hz, PCH_2N, chair-boat), 2.42 (dd, 0.5H, $^2J_{HH}$ = 11.8 Hz, $^2J_{HP}$ = 27.4 Hz, PCH_2N, chair-boat), 0.75 (d, 17.5H, $^3J_{HP}$ = 9.9 Hz, C(CH_3)$_3$, crown), 0.70 (br s, 4.1H, C(CH_3)$_3$, chair-boat). ^{31}P{^{1}H} NMR (THF-d_8, −50 °C): δ −37.5 (s, 0.5P, chair-boat), −62.3 (s, 2.0P, crown). Anal. Calcd for $C_{26}H_{40}N_2P_2$: C, 70.56; H, 9.11; N, 6.33. Found: C, 70.42; H, 9.21; N, 6.31.

[Co($P^{tBu}{}_2N^{Ph}{}_2$)(CH$_3$CN)$_3$](BF$_4$)$_2$. A solution of [Co(CH$_3$CN)$_6$](BF$_4$)$_2$ (459.6 mg, 0.96 mmol) in CH$_3$CN (3 mL) was added via pipet to a suspension of $P^{tBu}{}_2N^{Ph}{}_2$ (400.8 mg, 0.97 mmol) in CH$_3$CN (8 mL), resulting in a rapid color change to yellow-brown. After the mixture was stirred for 24 h, all of the solids had dissolved. The solution volume was concentrated in vacuo to a volume of ca. 4 mL, and then vapor diffusion of Et$_2$O (ca. 12 mL) into the solution afforded [Co($P^{tBu}{}_2N^{Ph}{}_2$)(CH$_3$CN)$_3$](BF$_4$)$_2$ (717.6 mg, 0.93 mmol, 97%) as dark brown crystals. Anal. Calcd for $C_{30}H_{45}B_2CoF_8N_5P_2$: C, 46.78; H, 5.89; N, 9.09. Found: C, 46.73; H, 5.91; N, 9.03. CV (0.2 M NEt$_4$BF$_4$ in CH$_3$CN, scan rate 100 mV/s): $E_{1/2}$, V vs Fc (ΔE_p, mV) +0.34 (114), −0.87 (63). μ_{eff} = 1.81 μ_B. UV−vis (CH$_3$CN): λ_{max} 456 nm (ε = 682 L cm^{-1} mol^{-1}).

[Co($P^{tBu}{}_2N^{Bz}{}_2$)(CH$_3$CN)$_3$](BF$_4$)$_2$. Solid [Co(CH$_3$CN)$_6$](BF$_4$)$_2$ (280.6 mg, 0.586 mmol) was added to a suspension of $P^{tBu}{}_2N^{Bz}{}_2$ (264.8 mg, 0.598 mmol) in CH$_3$CN (7 mL), resulting in a rapid color change to yellow-brown. After the mixture was stirred for 21 h, all of the solids had dissolved. The solution volume was concentrated in vacuo to a volume of ca. 4 mL, and then vapor diffusion of Et$_2$O (ca. 6 mL) into the solution afforded [Co($P^{tBu}{}_2N^{Bz}{}_2$)(CH$_3$CN)$_3$](BF$_4$)$_2$·CH$_3$CN (462.8 mg, 0.551 mmol, 94%) as dark brown crystals. Anal. Calcd for $C_{34}H_{52}B_2CoF_8N_6P_2$: C, 48.65; H, 6.24; N, 10.01. Found: C, 48.54; H, 6.26; N, 9.68. CV (0.2 M NEt$_4$BF$_4$ in CH$_3$CN, scan rate 100 mV/s): $E_{1/2}$, V vs Fc (ΔE_p, mV) +0.26 (161), −0.94 (82). μ_{eff} = 1.95 μ_B. UV−vis (CH$_3$CN): λ_{max} 443 nm (ε = 664 L cm^{-1} mol^{-1}).

[Ni($P^{tBu}{}_2N^{Ph}{}_2$)(CH$_3$CN)$_3$](BF$_4$)$_2$. The ligand $P^{tBu}{}_2N^{Ph}{}_2$ (0.100 g, 0.241 mmol) was combined with [Ni(CH$_3$CN)$_6$](BF$_4$)$_2$ (0.121 g, 0.241 mmol) in 6 mL of CH$_3$CN, and the mixture was stirred at room temperature for 2 days. The ligand was not initially soluble but mostly dissolved over the course of the reaction. The solution was then filtered to remove any remaining ligand, and the filtrate was reduced under vacuum to 2 mL and placed in a diffusion chamber with diethyl ether overnight. The product precipitated as red block crystals (0.120 g, 65%) and were isolated by filtration and washed with 2 × 2 mL of diethyl ether. Anal. Calcd for $C_{30}H_{45}B_2F_8N_5NiP_2$: C, 46.80; H, 5.89; N, 9.10. Found: C, 47.00; H, 5.86; N, 8.97. ^{1}H NMR (CD$_3$CN, +80 °C): δ 16.9 (br s, $\Delta\nu_{1/2}$ = 481 Hz, 4H, PCH$_2$N), 7.52 (t, 4H, $^3J_{HH}$ = 6.8 Hz, Ar *H*), 7.38 (d, 4H, $^3J_{HH}$ = 7.5 Hz, Ar *H*), 7.16 (t, 2H, $^3J_{HH}$ = 7.3 Hz, Ar *H*), 6.33 (br s, $\Delta\nu_{1/2}$ = 71 Hz, 4H, PCH$_2$N), 2.53 (br s, $\Delta\nu_{1/2}$ = 38 Hz, 18H, C(CH_3)$_3$), 1.96 (s, 9H, CH_3CN). ^{31}P{^{1}H} NMR (CD$_3$CN, −40 °C): δ 9.6 (br s). ^{1}H NMR (CD$_2$Cl$_2$): δ 7.55 (t, 4H, $^3J_{HH}$ = 8.0 Hz, Ar *H*), 7.28 (d, 4H, $^3J_{HH}$ = 8.2 Hz, Ar *H*), 7.21 (t, 2H, $^3J_{HH}$ = 7.4 Hz, Ar *H*), 4.26 (d, 4H, $^2J_{HH}$ = 14.3 Hz, PCH_AH$_B$N), 3.64 (d, 4H, $^2J_{HH}$ = 14.3 Hz, PCH$_A$$H_B$N), 2.23 (s, 9H, C$H_3$CN), 1.35 (s, 18H, C(C$H_3$)$_3$). ^{31}P{^{1}H} NMR (CD$_2Cl_2$): δ 11.9 (br s). CV (0.2 M NEt$_4$BF$_4$ in CH$_3$CN, scan rate 100 mV/s): $E_{1/2}$, V vs Fc (ΔE_p, mV) −0.59 (99), −1.48 (271).

[Ni($P^{tBu}{}_2N^{Bz}{}_2$)(CH$_3$CN)$_2$](BF$_4$)$_2$. The ligand $P^{tBu}{}_2N^{Bz}{}_2$ (0.200 g, 0.452 mmol) was combined with [Ni(CH$_3$CN)$_6$](BF$_4$)$_2$ (0.243 g, 0.586 mmol) in 6 mL of CH$_3$CN, and the mixture was stirred at room temperature for 2 h. The reaction solution was reduced to 3 mL under vacuum. The solution was put into a diffusion chamber with diethyl ether overnight, after which the product precipitated as red crystalline needles. The product was isolated by filtration and washed with 2 × 2 mL of diethyl ether (62%). Anal. Calcd for $C_{30}H_{46}B_2F_8N_4NiP_2$: C, 47.60; H, 6.13; N, 7.40. Found: C, 48.06; H, 6.23; N, 7.41. ^{1}H NMR (CD$_3$CN, +80 °C): δ 7.49 (d, 4H, $^3J_{HH}$ = 7.7 Hz, Ar *H*), 7.44 (t, 4H, $^3J_{HH}$ = 7.4 Hz, Ar *H*), 7.38 (t, 2H, $^3J_{HH}$ = 7.2 Hz, Ar *H*), 5.00 (br s, 3.5H, $\nu_{1/2}$ = 64 Hz, NCH_2Ph), 4.36 (s, 4H, PCH_2N), 3.61 (s, 2H, PCH_2N), 3.58 (s, 2H, PCH_2N), 1.96 (s, 5.5H, CH_3CN), 1.28 (s, 18H, C(CH_3)$_3$). ^{31}P{^{1}H} NMR (CD$_3$CN, −40 °C): δ −2.5 (br s). ^{1}H NMR (CD$_3$NO$_2$): δ 7.51 (d, 4H, $^3J_{HH}$ = 7.2 Hz, Ar *H*), 7.44 (t, 4H, $^3J_{HH}$ = 7.3 Hz, Ar *H*), 7.38 (t, 2H, $^3J_{HH}$ = 7.2 Hz, Ar *H*), 4.49 (br s, 4H, NCH_2Ph), 3.53 (br s, 8H, PCH_2N), 2.42 (br s, 6H, CH_3CN), 1.23 (br s, 18H, C(CH_3)$_3$). ^{31}P{^{1}H} NMR (CD$_2$NO$_2$): δ 5.3 (br s). CV (0.2 M NEt$_4$BF$_4$ in MeCN, scan rate 100 mV/s): $E_{1/2}$, V vs Fc (ΔE_p, mV) −0.69 (104), −1.53 (irrev).

Acid Dependence. General Procedure. A 1.5 mL portion of a 0.0020 M solution of catalyst in 0.2 M NEt$_4$BF$_4$/CH$_3$CN containing ferrocene as a reference was syringed into a CV cell. An initial CV was obtained with a scan rate of 50 mV/s. A 0.50 M solution of acid in 0.2 M NEt$_4$BF$_4$/CH$_3$CN was then added in sequential aliquots (20 × 15 μL, 3−4 × 150 μL) with a CV being obtained after each addition. The current intensity of the Fc anodic wave was used as an internal reference to adjust the values for i_p and [acid] to compensate for sample dilution as the acid solution was introduced.

Acid-Independent Rate. A 1.0 mL portion of a 0.0010 M solution of catalyst in 0.2 M NEt$_4$BF$_4$/CH$_3$CN containing ferrocene as a reference was syringed into a CV cell. An initial CV was obtained with a scan rate of 50 mV/s. A 1.0 M solution of 4-bromoanilinium tetrafluoroborate in 0.2 M NEt$_4$BF$_4$/CH$_3$CN was then added in sequential aliquots (4 × 50 μL, 4 × 100 μL, 1 × 300 μL) with a CV being obtained after each addition. The current intensity of the Fc anodic wave was used as an internal reference to adjust the values for i_p and [acid] to compensate for sample dilution as the acid solution was introduced. Two separate runs were averaged to obtain the plot shown in Figure 6.

Catalyst Concentration Dependence for [Co($P^{tBu}{}_2N^{Ph}{}_2$)(CH$_3$CN)$_3$](BF$_4$)$_2$. A 1.5 mL portion of an acetonitrile solution that was 0.1 M in 4-bromoanilinium tetrafluoroborate and 0.2 M in NEt$_4$BF$_4$ containing a ferrocene reference was syringed into a CV cell. Sequential aliquots from a solution that was 0.020 M in [Co($P^{tBu}{}_2N^{Ph}{}_2$)(CH$_3$CN)$_3$](BF$_4$)$_2$ in 0.2 M NEt$_4$BF$_4$/CH$_3$CN were syringed into the CV cell (6 × 20 μL), with a CV being recorded after each addition.

Bulk Electrolysis. A three-necked flask with a stopcock was used for a bulk electrolysis experiment. One neck was a 24/40 joint that accepted a rubber septum through which two lengths of copper wire were fed. One wire was attached to a 1 mm PEEK-encased glassy-carbon electrode for CV measurement, and the second wire was attached to a cylinder of reticulated vitreous carbon as a working electrode for bulk electrolysis. The other two necks of the flask were 14/20 joints. Both were fitted with glass compartments with Vycor frits on the bottom. One was used as the reference electrode—it was filled with a 0.2 M NEt$_4$BF$_4$ acetonitrile solution and a silver wire. The other compartment was used as the counter electrode, and it contained a 0.2 M NEt$_4$BF$_4$ acetonitrile solution and a Ni−Cr wire. With these fittings attached, the cell had a total volume of 149 mL. The cell was filled from stock solutions to give 18 mL of an acetonitrile solution that was 0.0010 M in [Co($P^{tBu}{}_2N^{Ph}{}_2$)(CH$_3$CN)$_3$](BF$_4$)$_2$, 0.230 M in 4-bromoanilinium tetrafluoroborate,

Table 4. Crystallographic Data for $[Co(P^{tBu}_2N^{Ph}_2)(CH_3CN)_3](BF_4)_2$, $[Co(P^{tBu}_2N^{Bz}_2)(CH_3CN)_3](BF_4)_2$, $[Ni(P^{tBu}_2N^{Ph}_2)(CH_3CN)_3](BF_4)_2$, and $[Ni(P^{tBu}_2N^{Bz}_2)(CH_3CN)_2](BF_4)_2$

	$[Co(P^{tBu}_2N^{Ph}_2)(CH_3CN)_3](BF_4)_2$	$[Co(P^{tBu}_2N^{Bz}_2)(CH_3CN)_3](BF_4)_2 \bullet CH_3CN$	$[Ni(P^{tBu}_2N^{Ph}_2)(CH_3CN)_3](BF_4)_2$	$[Ni(P^{tBu}_2N^{Bz}_2)(CH_3CN)_2](BF_4)_2$
empirical formula	$C_{30}H_{45}B_2CoF_8N_5P_2$	$C_{34}H_{52}B_2CoF_8N_6P_2$	$C_{30}H_{45}B_2F_8N_5NiP_2$	$C_{30}H_{46}B_2F_8N_4NiP_2$
mass (amu)	770.20	839.31	769.98	756.98
cryst syst	monoclinic	monoclinic	monoclinic	orthorhombic
space group	$P2_1/c$	$P2_1/n$	$P2_1/c$	$P2_12_12_1$
a (Å)	10.8564(11)	10.2216(3)	10.7444(4)	11.4437(2)
b (Å)	22.783(2)	18.3939(5)	22.7008(8)	16.1666(2)
c (Å)	14.3551(15)	22.2016(6)	14.5661(5)	19.2126(3)
α (deg)	90	90	90	90
β (deg)	94.948(2)	102.0710(10)	94.1870(10)	90
γ (deg)	90	90	90	90
V (Å^3)	3537.4(6)	4081.9(2)	3543.3(2)	3554.44(9)
Z	4	4	4	4
T (K)	100(2)	100(2)	100(2)	100(2)
R index[a] ($I > 2\sigma(I)$)	R1 = 0.0411, wR2 = 0.0918	R1 = 0.0409, wR2 = 0.0913	R1 = 0.0533, wR2 = 0.0910	R1 = 0.0405, wR2 = 0.0894
R index[a] (all data)	R1 = 0.0678, wR2 = 0.1026	R1 = 0.0681, wR2 = 0.1015	R1 = 0.1184, wR2 = 0.1083	R1 = 0.0558, wR2 = 0.0958
weighting coeff[b]	a = 0.0459, b = 0.4739	a = 0.0446, b = 0.9880	a = 0.0370, b = 0	a = 0.0525, b = 0.2627
GOF[c] on F^2	1.020	1.034	1.012	1.010

[a] $R1 = \sum||F_o| - |F_c||/\sum|F_o|$; $wR2 = [\sum w(F_o^2 - F_c^2)/\sum w(F_o^2)^2]^{1/2}$. [b] $w^{-1} = [\sigma^2(F_o^2) + (ap)^2 + bp]$, where $p = (F_o^2 + 2F_c^2)/3$. [c] $GOF = S = [\sum w(F_o^2 - F_c^2)/(M - N)]^{1/2}$, where M is the number of reflections and N is the number of parameters refined.

and 0.2 M in NEt_4BF_4. The solution also contained a small amount of ferrocene as a reference. Controlled-potential coulometry was performed at −1.11 V versus the ferrocenium/ferrocene couple. After 42.01 C of charge was applied, samples of the gas in the flask headspace were removed via a gastight syringe and analyzed by gas chromatography. The percentage of hydrogen and nitrogen in the headspace were determined through calibration against gas standards of known composition. The total amount of hydrogen produced was calculated as the sum of the hydrogen in the headspace and the sum of the hydrogen dissolved in the solvent, as determined from Henry's law.[35] From these data 11.7 mol of H_2 was produced per mole of catalyst, and a current efficiency of 96 ± 5% was calculated for H_2 production.

Catalyst Stability. General Procedure. An H-shaped glassware assembly was used in which one leg was a graduated tube and the other leg was a cuvette with a 10 mm path length. Each leg of the H shape was sealed at the top with a Teflon valve. A solution of the appropriate acid in CH_3CN was measured into the graduated leg, while a solution of $[Co(P^{tBu}_2N^{Ph}_2)(CH_3CN)_3](BF_4)_2$ in CH_3CN was measured into the cuvette leg. The two solutions were mixed to give final concentrations of 1 mM catalyst and 75 mM acid, and then the solution was monitored immediately by UV−vis at 456 nm with measurements recorded every minute. At the end of the kinetic experiment, a full UV−vis spectrum was recorded and compared to the spectrum of $[Co(CH_3CN)_6](BF_4)_2$ (λ_{max} 472 nm): 4-bromoanilinium tetrafluoroborate, final λ_{max} 457 nm; 4-cyanoanilinium tetrafluoroborate, final λ_{max} 470 nm; 2,6-dichloroanilinium tetrafluoroborate, final λ_{max} 472 nm. The measured absorbances were corrected for the background absorbance of the solvent, and then the concentration of **2-Ph** was determined at each time interval using the Beer−Lambert law. Assuming that the decay was first-order in **2-Ph**, the rate of decay (k) was determined from the slope of a plot of ln[**2-Ph**] vs time, and then the half-life was calculated as $\ln 2/k$.

X-ray Diffraction Studies. For each of the crystal structure studies, a single crystal was mounted using NVH immersion oil onto a nylon fiber and cooled to the data collection temperature of 100(2) K. Data were collected on a Brüker-AXS Kappa APEX II CCD diffractometer with 0.710 73 Å Mo Kα radiation. The data sets were treated with SADABS absorption corrections based on redundant multiscan data.[36] In the structures of $[Co(P^{tBu}_2N^{Ph}_2)(CH_3CN)_3](BF_4)_2$, $[Ni(P^{tBu}_2N^{Ph}_2)(CH_3CN)_3](BF_4)_2$, and $[Ni(P^{tBu}_2N^{Bz}_2)(CH_3CN)_2](BF_4)_2$ one of the anions was disordered over two positions, which were located from the difference map and restrained to be chemically equivalent. All non-hydrogen atoms were refined with anisotropic displacement parameters. All hydrogen atoms were treated as idealized contributions. Additional details of the structural studies are given in Table 4 and in the Supporting Information.

Acknowledgment. We thank the U.S. Department of Energy, Office of Science, Office of Basic Energy Sciences, Division of Chemical Sciences, Biosciences and Geosciences, for support of the cobalt chemistry reported here. The nickel chemistry was supported as part of the Center for Molecular Electrocatalysis, an Energy Frontier Research Center funded by the U.S. Department of Energy, Office of Science, Office of Basic Energy Sciences. Pacific Northwest National Laboratory is operated by Battelle for the U.S. Department of Energy.

Supporting Information Available: CIF files giving crystallographic data for complexes **2-Ph, 2-Bz, 3-Ph,** and **3-Bz**, figures giving 2D and variable-temperature NMR spectra, details of MM2 calculations and tables of XYZ coordinates for optimized $P^{tBu}_2N^{Ph}_2$ conformers, and additional cyclic voltammetry plots. This material is available free of charge via the Internet at http://pubs.acs.org.

(35) Purwanto; Deshpande, R. M.; Chaudhari, R. V.; Delmas, H. *J. Chem. Eng. Data* **1996**, *41*, 1414–1417.

(36) *SADABS version 2001/1: an Empirical Absorption Correction Program*; Bruker AXS Inc., Madison, WI, 2001.